Inorganic Chemistry

Article

pubs.acs.org/IC

Activation of Dimanganese Class Ib Ribonucleotide Reductase by Hydrogen Peroxide: Mechanistic Insights from Density Functional Theory

Katarina Roos* and Per E. M. Siegbahn

Department of Physics, Stockholm University, SE-106 91 Stockholm, Sweden

Supporting Information

ABSTRACT: Activation of manganese-dependent class Ib ribonucleotide reductase by hydrogen peroxide was modeled using B3LYP* hybrid density functional theory. Class Ib ribonucleotide reductase R2 subunit (R2F) does not react with molecular oxygen. Instead R2F is proposed to react with H_2O_2 or HO_2^-, provided by the unusual flavodoxin protein NrdI, to generate the observed manganese(III) manganese(III) tyrosyl-radical state. On the basis of the calculations, an energetically feasible reaction mechanism is suggested for activation by H_2O_2, which proceeds through two reductive half-reactions. In the first reductive half-reaction, H_2O_2 is cleaved with a barrier of 13.1 kcal mol^{-1} [Mn(II)Mn(II) → Mn(III)Mn(III)], and in the second reductive half-reaction, H_2O_2 is cleaved with a barrier of 17.0 kcal mol^{-1} [Mn(III)Mn(III) → Mn(IV)Mn(IV)]. Tyrosyl-radical formation from both the Mn(IV)Mn(IV) state and a Mn(III)Mn(IV) state, where an electron and proton have been taken up, is both kinetically and thermodynamically accessible. Hence, chemically, H_2O_2 is a possible oxidant for the manganese-dependent R2F. The selectivity between the second reductive half-reaction and a competing oxidative reaction, as in manganese catalase, may be the time scale for the availability of H_2O_2. The role of NrdI may be to provide H_2O_2 on the correct time scale.

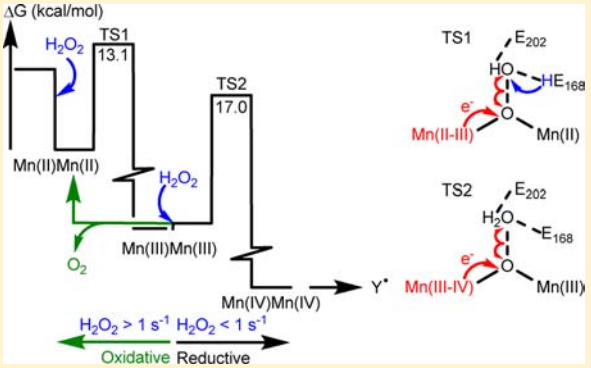

1. INTRODUCTION

Ribonucleotide reductase (RNR) catalyzes the reduction of ribonucleotides, the building blocks for RNA, to deoxyribonucleotides, the building blocks for DNA. There are three classes of RNR, depending on their redox cofactors. Class I RNR consists of two subunits: R1, the catalytic subunit that contains the active site for substrate reduction, and R2, the subunit that contains the metal cofactor that generates, stores, and delivers a radical essential for the substrate reduction. Class I is further divided into three different subclasses, class Ia, Ib, and Ic, depending on the metal cofactor.[1−6]

The metal cofactor of class Ia R2 has a diiron center and is oxidized by reductive cleavage of dioxygen (O_2; Scheme 1). An electron is taken up from a neighboring tryptophan during or just after oxygen cleavage. The product is an Fe(III)Fe(IV) state known as compound X. Compound X is responsible for formation of a radical at a neighboring tyrosine. The radical is transferred to the catalytic subunit R1, where the substrate reduction is catalyzed, and is thereafter transferred back to the tyrosine in R2, where it is stored for the next substrate reduction cycle.

Class Ic R2 (R2c) lacks the radical-bearing tyrosine that is crucial for activity in class Ia and Ib RNRs.[9,10] Instead, the R2c active cofactor contains a Mn(IV)Fe(III) metal center.[11,12] The active state is generated by reductive oxygen cleavage at the metal site (Scheme 1). The product is a Mn(IV)Fe(IV) state.[13] The Mn(IV)Fe(IV) state is thereafter reduced to the active Mn(IV)Fe(III) state by uptake of an electron, from a tyrosine near the surface, via a neighboring tryptophan.[14] The Mn(IV)Fe(III) active state is responsible for delivering the radical for the substrate reduction in R1. The role of the metal center is to provide the correct redox potential to enable reversible radical transfer. In the absence of the tyrosyl radical, an equally strong oxidant is needed. In earlier work, the Mn(IV)Fe(III) active state in R2c was shown to have the same redox potential as that of the tyrosyl radical in class Ia R2.[15] A diiron state with Fe(III)Fe(IV) has a too high redox potential and would lead to an inactive R2c.

The nature of the metal center of class Ib R2 (R2F) has been under debate. The situation is summarized in three recent reviews.[5,6,16] The native RNR from *Corynebacterium ammoniagenes* was earlier proposed to use manganese instead of iron for enzymatic function.[17−20] This contrasted with the observation of an active R2F with a diiron site when the gene was expressed in *Escherichia coli*, which led to the proposal that the *C. ammoniagenes* RNR is a class Ib RNR with a diiron metalloradical cofactor.[20−22] Recently, the consensus was reached that the manganese form of class Ib R2F is relevant in vivo for most organisms[7,8] (Scheme 1). This is supported by

Received: April 24, 2012
Published: March 28, 2013

dx.doi.org/10.1021/ic3008427 | Inorg. Chem. 2013, 52, 4173−4184

Scheme 1. Schematic View of Differences and Similarities of the Activation and Role of the Metal Center in Classes Ia R2a, Ic R2c, and Ib R2F and MnCat[a]

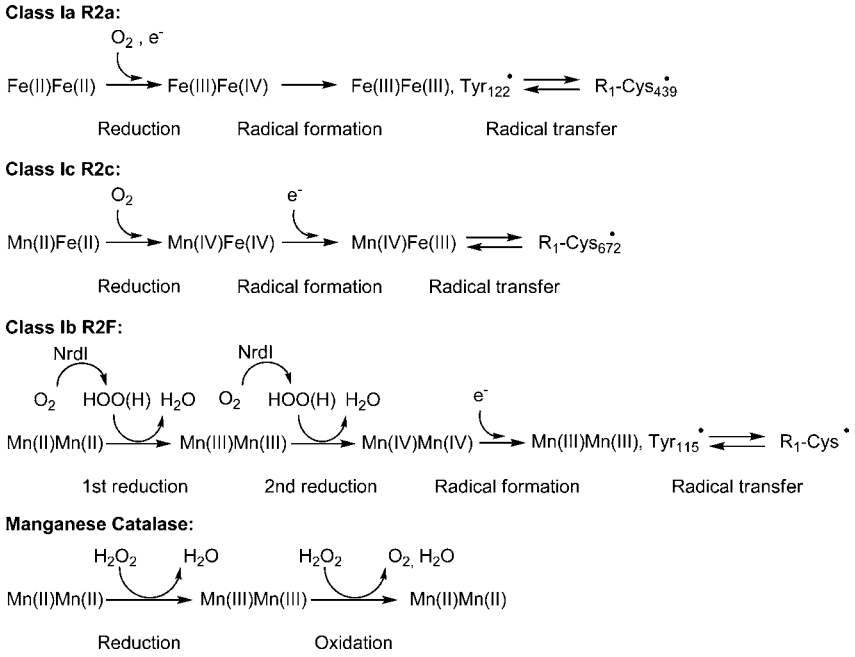

[a]The activation mechanism of R2F is hypothetical.[7,8] *E. coli* numbering for R2a, *Chlamydia trachomatis* numbering for R2c, and *C. ammoniagenes* numbering for R2F.

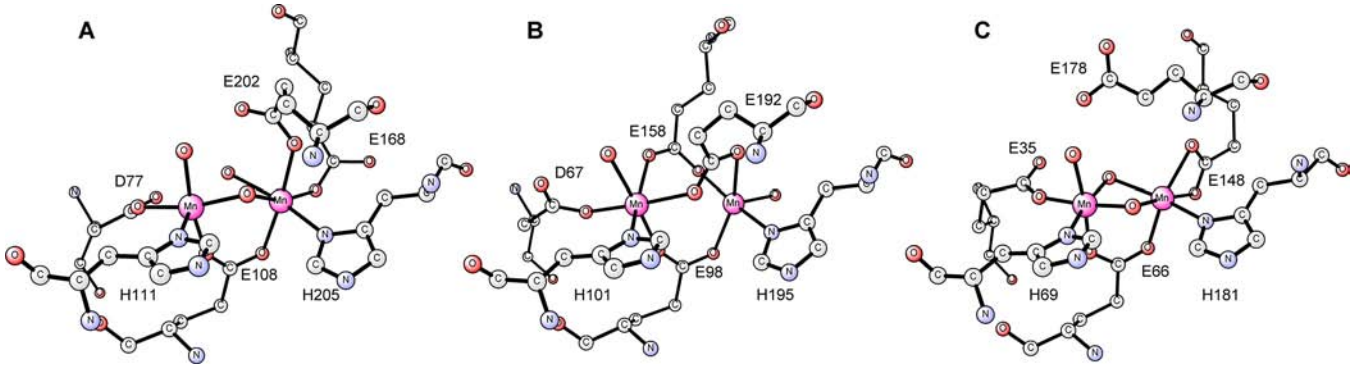

Figure 1. Comparison of the active site structures of class Ib RNR and MnCat. (A) Structure of oxidized manganese-dependent R2F from *C. ammoniagenes*, PDB id 3MJO.[8] (B) Structure of reduced manganese-dependent R2F from *E. coli*, PDB id 3N37.[31] (C) Structure of oxidized MnCat from *Lactobacillus plantarum*, PDB id 1JKU.[38]

several observations, for example, the observation of *E. coli* R2F with a dimanganese center and a tyrosyl radical in vitro[7] and in vivo,[23,24] the crystal structure and electron paramagnetic resonance measurements of *C. ammoniagenes* R2F showing that the in vivo metalloradical cofactor contains a dimanganese center and a tyrosyl radical (Figure 1A),[8,25] an active native R2F from *Corynebacterium glutamicum* with a dimanganese center and a tyrosyl radical,[26] an active dimanganese center with a tyrosyl radical in R2F natively expressed in *Bacillus subtilis*,[27] and the fact that the manganese forms of R2Fs from *Bacillus anthracis*,[28] *E. coli*,[7] and *B. subtilis*[27] were 10-fold more active than the iron forms.

Class Ib RNR in *E. coli* is expressed under oxidative stress and iron starvation, giving a rationalization to the manganese dependence. The dimanganese *E. coli*, *C. ammoniagenes*, and *Salmonella typhimurium* R2Fs do not react with molecular oxygen.[7,22] In a previous article, oxygen cleavage with the iron and manganese R2 homodimers and heterodimer was investigated by density functional theory (DFT).[29] Oxygen cleavage was found to be governed by two factors: the redox potentials of the metals and the relative stability of the different peroxides. Mn(IV) has a lower redox potential than Fe(IV), or, equivalently, Mn(III) is easier to oxidize than Fe(III), and the barrier is therefore lower with a mixed-metal center than with a diiron center. With a dimanganese center, an end-on asymmetric peroxide is more stable than a symmetric peroxide, and the barrier for oxygen cleavage therefore becomes too high, providing a rationalization for the inability of the dimanganese R2F to activate oxygen.[29]

Instead, R2F is proposed to react with hydrogen peroxide (H_2O_2) or HO_2^- to generate the tyrosyl radical.[7] This is supported by the activity dependence on the flavodoxin NrdI[7,23,30] and the crystal structure of *E. coli* R2F, where the NrdI cofactor is docked with immediate access through a channel to the active dimanganese center.[31] NrdI is an unusual flavodoxin protein that is encoded in the same operon as NrdE

dx.doi.org/10.1021/ic3008427 | *Inorg. Chem.* 2013, 52, 4173−4184

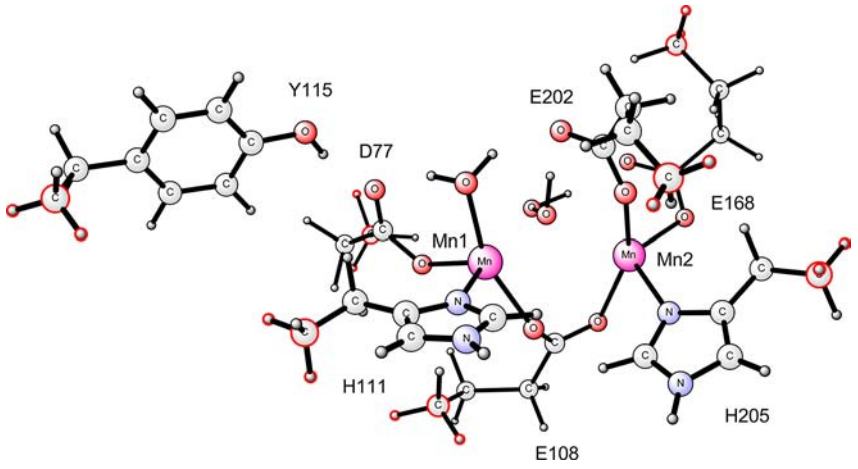

Figure 2. Chemical model of the active site of class Ib R2F, based on the crystal structure of *C. ammoniagenes* RNR subunit II, PDB id 3MJO.[8] Atoms marked with red empty circles are fixed in the calculations.

and NrdF, the two components of the class Ib RNR.[32−34] The role of NrdI in metalloradical cofactor biosynthesis is proposed to be to provide oxidizing equivalents, derived from O_2, such as H_2O_2, HO_2^-, or $O_2^{\bullet-}$, to the reduced manganese complex. It has been argued that the oxidant is HO_2^-, based on the in vitro observations that neither H_2O_2 nor O_2 activates the cofactor assembly without NrdI[7,22] and that the level of $O_2^{\bullet-}$ production by reaction of NrdI with O_2 is not sufficient to account for the amount of $Tyr^{\bullet}$ generated.[7] The addition of H_2O_2 to the reduced dimanganese *C. ammoniagenes* R2F, without NrdI, leads to oxidation of the cluster but no tyrosyl-radical formation.[22] After quenching of the tyrosyl radical by hydroxyurea, the tyrosyl radical can be regenerated in the absence of NrdI by the addition of H_2O_2 in conjunction with methylviologen as a mediator.[8] It has also been argued that NrdI might affect the structure or redox properties of NrdF and that H_2O_2 could therefore still be the oxidant.[6] In addition, the MnFe heterodimer in class Ic R2c can be efficiently activated by H_2O_2.[35] The reaction of the reduced Mn(II)Fe(II) state with H_2O_2 proceeds in three resolved steps: first oxidation to Mn(III)Fe(III), followed by oxidation to Mn(IV)Fe(IV), and finally electron uptake and decay to the Mn(IV)Fe(III) active state.

A similar mechanistic pathway for activation of the dimanganese R2F that involves two discrete oxidation steps using H_2O_2/HO_2^- is proposed.[7,8] The first reductive half-reaction is similar to the dismutation reaction in manganese catalase (MnCat)[8,36,37] (Scheme 1). MnCat is a four-helix bundle carboxylate protein with a dimanganese center, similar to R2F (Figure 1C).[38] MnCat catalyzes the disproportionation of H_2O_2 into water (H_2O) and O_2. The metal cofactor cycles between a reduced Mn(II)Mn(II) state and an oxidized Mn(III)Mn(III) state during turnover. The reaction starts from a Mn(II)Mn(II) state. In the first reductive half-reaction, one H_2O_2 is reduced, forming H_2O and a μ-OH_x-bridged Mn(III)Mn(III) state, similar to the suggestion for R2F.[7,8] In the second oxidative half-reaction, a second H_2O_2 is oxidized, forming H_2O, O_2, and a Mn(II)Mn(II) state. Hence, the second half-reaction is distinctly different in MnCat (oxidative) and R2F (reductive) (Scheme 1). Insights into specificity can be gained by studying the activation of R2F with H_2O_2 and comparing it with MnCat.

In the present work, H_2O_2 reduction and tyrosyl-radical formation in class Ib R2F are modeled with DFT, and a feasible reaction mechanism is suggested. Comparisons with MnCat are made.

2. COMPUTATIONAL METHODS

The calculations were performed in three steps, using *Jaguar 7.6*[39] and unrestricted DFT with the B3LYP* hybrid exchange-correlation functional, where 15% Hartree−Fock exchange is used instead of 20% as in B3LYP.[40,41] An accuracy of 3−5 kcal mol^{-1} can be expected for computed relative energies of transition-metal-containing systems, based on tests of the B3LYP functional.[42] With the B3LYP* functional, the good accuracy of B3LYP on standard benchmarks is maintained, and the performance on metal complexes in weak ligand fields is improved.[43]

In the first step, the geometries were optimized using B3LYP and a standard double-ζ basis set (LACVP*) with an effective core potential on the metals.[44] In the second step, accurate energies in the optimized structures were calculated, using B3LYP* with a triple-ζ basis set [ccpVTZ(-f)].[45−47] A triple-ζ basis set with diffuse functions (LACV3P+) was used to treat the metals. The electrostatic solvation effects from the surrounding protein were calculated in the third step, using a standard Poisson−Boltzmann solver,[48,49] with a dielectric constant of 4.0 in line with previous modeling of enzymes.[50]

Transition state optimizations were performed using *Gaussian 03*, with the LACVP* basis set imported from *Jaguar*.[51] The transition states were considered optimized when the root-mean-square (rms) force was less than 3×10^{-4} hartree/(bohr, radian). By visualization, the largest imaginary frequency was concluded to correspond to the correct reaction coordinate. In order to account for the strain from the surrounding protein on the amino acids included, three atoms on each amino acid were fixed: the α-carbon and two hydrogen atoms along the backbone. Because fixed coordinates were used, there were more than one imaginary frequency in the optimized transition states, however smaller and clearly corresponding to each fixed group of atoms.

The second derivatives were calculated for all optimized structures to obtain zero-point corrections. Because some coordinates are being held fixed, entropy contributions cannot be calculated. In the reaction steps involving the addition or removal of a small molecule (H_2O, H_2O_2, and O_2), where the relative entropy contributions are substantial, an empirical correction term is included to account for the experimental solvation free energy of the small molecule in solution and the entropy loss upon binding to the protein. For O_2 removal, an entropy gain of 10.8 kcal mol^{-1} was included, corresponding to the calculated translational entropy of O_2 in the gas phase. The calculated translational entropy in the gas phase is 10.9 kcal mol^{-1} for H_2O_2 and 10.3 kcal mol^{-1} for H_2O, and the aqueous solvation free energy is 8.6 kcal mol^{-1} for H_2O_2 and 6.3 kcal mol^{-1} for H_2O.[52,53] On the basis of an empirical experience, a correction term of

dx.doi.org/10.1021/ic3008427 | *Inorg. Chem.* 2013, 52, 4173−4184

Scheme 2. Proposed Reaction Scheme for the First Reductive Half-Reaction[a]

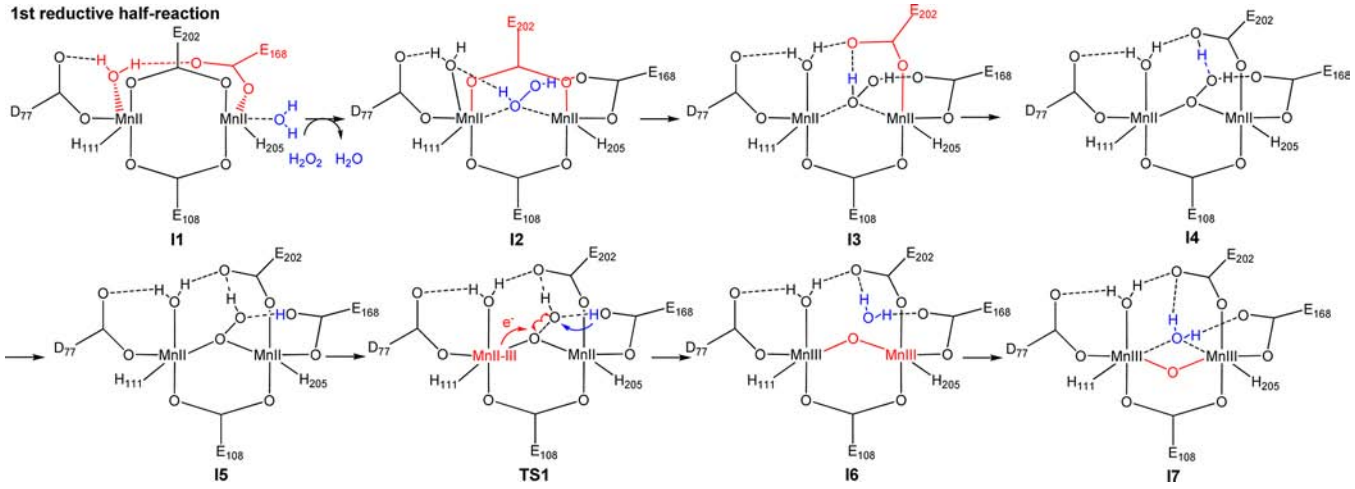

[a] *C. ammoniagenes* numbering.

14.0 kcal mol^{-1} was used for H_2O addition, corresponding to the assumption that a H_2O molecule keeps approximately 2.6 kcal mol^{-1} of the translational entropy in the protein.[54] Assuming the same value of 2.6 kcal mol^{-1} for H_2O_2, the corresponding correction term is 16.9 kcal mol^{-1}.

The inability to describe long-range electron correlations that are responsible for van der Waals forces is a general drawback of hybrid DFT.[55] Dispersion corrections were calculated through the empirical formula of Grimme and applied on top of the energies calculated with B3LYP*.[55] The energy values presented throughout the manuscript include solvation effects, zero-point corrections, empirical entropy effects, and dispersion corrections. The states with antiferromagnetically coupled metals may be corrected for the broken-symmetry state, using Noodleman's protocol.[56] However, the corrections were found to be so small (see below) that they were not included.

2.1. Models. The quantum-chemical calculations were performed on a chemical model of the protein consisting of the active site complex. A model of the active site was constructed from the coordinates of the X-ray crystal structure of *C. ammoniagenes* R2F (PDB id 3MJO; Figure 2).[8] The metals, first-shell ligands, and tyrosine were included in the model. Calculations were made on two models, a neutral structure (Figure 2) and a positively charged one, where the aspartate D77 is protonated.[8]

This type of cluster model has previously been employed to successfully study a large number of enzymatic systems.[57] There have been several studies of the convergence of the cluster model, showing that at a certain size of the model the results are no longer dependent on the surrounding continuum solvation model.[58−61] Studies showing a lack of convergence for the cluster model all have in common that the geometry was not optimized.[62,63] The size of the cluster model in the present work may not be fully converged, and there may therefore be effects from the surrounding protein outside of the model; however, they are not expected to be significant.

3. RESULTS AND DISCUSSION

The reaction mechanism investigated is based on the suggestion in refs 7 and 8. In the first reductive half-reaction, one H_2O_2 is reduced and the metal center is oxidized, forming a Mn(III)Mn(III) state and H_2O. In the second reductive half-reaction, a second H_2O_2 is reduced and the metal center is oxidized, forming a Mn(IV)Mn(IV) state and H_2O. The Mn(IV)Mn(IV) state may be responsible for forming the radical on the neighboring tyrosine. The tyrosyl radical observed is coupled to a ferromagnetically coupled Mn(III)-Mn(III) state, indicating that an extra electron should be taken up either before or after formation of the radical. A comparison of the second reductive half-reaction and the corresponding oxidative half-reaction in MnCat will be discussed in the last part of the section.

In all intermediates calculated, the metals are high-spin Mn(II) ($S = {}^5/_2$), Mn(III) ($S = 2$), and Mn(IV) ($S = {}^3/_2$) and antiferromagnetically coupled. The energy differences between the broken-symmetry states and the corresponding ferromagnetic states are between 0 and 1.2 kcal mol^{-1}. In the weak coupling regime, DFT often cannot correctly reproduce the sign of the exchange coupling. The correction for the broken symmetry is even smaller.[56] The broken-symmetry energies are therefore used throughout the rest of the present study.

3.1. First Reductive Half-Reaction. *3.1.1. Reduced Mn(II)Mn(II) State.* The first reductive half-reaction starts from a reduced Mn(II)Mn(II) state. A possible reduced state is similar to the X-ray crystal structure of the reduced dimanganese *C. ammoniagenes* R2F.[21] The addition of H_2O_2 to this reduced state to form intermediate I3 is exergonic with 7.7 kcal mol^{-1}. Another possible reduced state is similar to the recently published X-ray crystal structure of the reduced dimanganese *E. coli* R2F, in which the glutamate E168 (*C. ammoniagenes* numbering when nothing else is stated) binds in an unusual bridging position between the two manganese atoms, trans to the two histidine ligands (Figure 1B).[31] The backbone position of E168 in the crystal structure of the reduced *E. coli* R2F Mn(II)Mn(II) state is slightly different from the one in the crystal structure of the oxidized *C. ammoniagenes* R2F Mn(III)Mn(III) state (Figure 1A), which is used to make a model of the active site (Figure 2).[8] To simplify energetic comparisons, the same crystal backbone structure was used throughout the present study. The exact position of E168 found in the crystal structure of reduced *E. coli* Mn(II)Mn(II) cannot be reached with the backbone position of E168 taken from the oxidized structure because of strain. E168 was therefore released, the backbone carbon atom was allowed to move, and the structure found in the X-ray crystal structure of the reduced *E. coli* R2F could be reached (I1 in Figure 1 in the Supporting Information). The position of the released E168 in the structure of the Mn(II)Mn(II) state with bound H_2O_2 (I4 in Scheme 2 and Figure 1 in the Supporting Information) is similar to the position in the X-ray crystal structure of *C.*

dx.doi.org/10.1021/ic3008427 | *Inorg. Chem.* 2013, 52, 4173−4184

ammoniagenes R2F Mn(III)Mn(III). The slightly different possible reduced structures should not affect the conclusions drawn about the suggested mechanism because the subsequent addition of H_2O_2 is exergonic both from a state resembling the reduced *E. coli* crystal structure, with both the fixed backbone position of E168 and released E168 (Figure 1 in the Supporting Information), and from a state that is similar to the crystal structure of the reduced *C. ammoniagenes* R2F.

3.1.2. Binding of H_2O_2. In the first step of the reaction, a H_2O molecule is released and H_2O_2 binds to the metal center (Scheme 2). Binding of H_2O_2 to the manganese in site 2 (Mn2 in Figure 2) is proposed based on the crystal structures of ions bound to MnCat.[38] Reorganization of the H_2O_2 ligand to the most stable binding mode will occur, which is with one of the oxygen atoms in a bridging position between the metals. The glutamate E202 is binding in a bridging position in the reduced state but opens up when H_2O_2 is added and binds monodentate to Mn2. The second oxygen atom of E202 accepts a hydrogen bond from the terminal H_2O on the manganese in site 1 (Mn1 in Figure 2). The binding of H_2O_2 is stabilized by one hydrogen bond to E168 and one hydrogen bond to E202 (I3) (Scheme 2). H_2O_2 is exergonically bound to the metal center (Figure 3 and Figure 1 in the Supporting Information). Without including dispersion, H_2O_2 is unbound (Figure 2 in the Supporting Information).

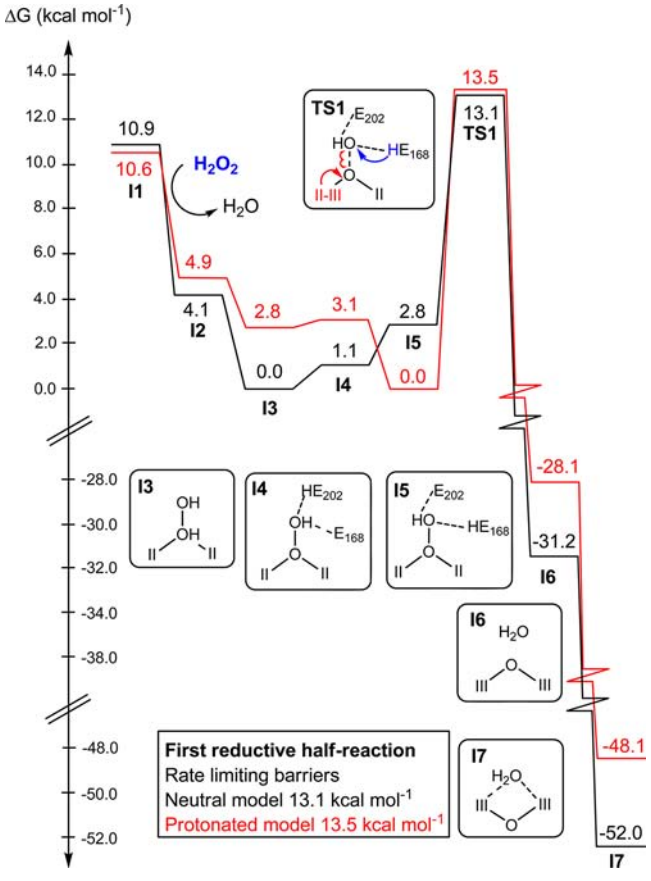

Figure 3. Energy profile for the first reductive half-reaction with a neutral model (black line) and a model in which D77 is protonated (red line). All values include solvation effects, zero-point corrections, empirical entropy corrections, and dispersion corrections. *C. ammoniagenes* numbering.

3.1.3. Deprotonation of H_2O_2. Both E202 and E168 are possible bases for the reaction. In the present mechanism, the bridging H_2O_2 protonates E202 (I4) and the hydrogen bond is changed from the bridging oxygen atom to the nonbridging oxygen atom (Scheme 2). From here, there can be an interchange of base, with a reprotonation of the substrate from E202 and then a protonation of E168 (I5). The energy difference between a protonated E202 and a protonated E168 is small, 1.7 kcal mol^{-1}, with E202 being the slightly better base (Figure 3). In the positively charged model where the aspartate D77 is protonated, as suggested in ref 8, E168 is instead the slightly better base with 3.1 kcal mol^{-1} (Figure 3).

3.1.4. Cleavage of H_2O_2. In the first transition state (TS1), the O−OH bond is cleaved homolytically at a distance of 1.93 Å (Figure 4). One electron is transferred from the manganese in site 1 (Mn1 in Figure 2) to the oxo bridge, and the metal is oxidized from Mn(II) to Mn(III). In the transition state, there is a concerted proton transfer from the base to the nonbridging oxygen atom. The reaction proceeds through an unstable Mn(III)Mn(II) state with an OH radical and the proton halfway between the base E168 and $OH^{\bullet}$. The positive charge of the proton attracts an electron from the oxo bridge. An electron transfer from the manganese in site 1 (Mn1 in Figure 2) to the oxo bridge occurs without a barrier, and the product is a Mn(III)Mn(III) state with a H_2O molecule (I6). The calculated barrier for the cleavage is 13.1 kcal mol^{-1} (13.5 kcal mol^{-1} in the protonated model), and the reaction is highly exergonic (Figure 3). The Mn(III)Mn(III) state with the oxo bridge on the same side as the histidines and the H_2O molecule directly coordinating to the metals (I7) is considerably lower than the corresponding state with the oxo bridge trans to the histidines and the H_2O molecule only hydrogen bonding to the carboxylates (I6). A mechanism where the O−OH bond is instead cleaved between the metals, in a bis(μ-oxo) structure, was examined in the protonated model and was found to have a higher barrier, 16.1 kcal mol^{-1}.

The rate constants for the reactions of the Mn(II)Mn(II) and Mn(III)Mn(III) forms of R2F with H_2O_2 are unknown. For comparison, the oxidation of R2c Mn(II)Fe(II) to Mn(III)Fe(III) by H_2O_2 has a second-order rate constant of 1.7 ± 0.3 mM^{-1} s^{-1} at 5 °C.[35] The barrier for H_2O_2 cleavage should be lower than 13 kcal mol^{-1}, corresponding to the apparent first-order rate constant at the highest measured concentration of H_2O_2 of 150 mM. In the transition state, only one metal is redox-active, in R2F being oxidized from Mn(II) to Mn(III). In the corresponding transition state for the mixed MnFe center in R2c, the redox-active metal could be either manganese or iron.

3.2. Second Reductive Half-Reaction. *3.2.1. Binding of H_2O_2.* The second reductive half-reaction starts from the Mn(III)Mn(III) state (I7) (Scheme 3). The H_2O molecule in a bridging position is replaced by a second H_2O_2. H_2O_2 binds with approximately equal strength to the complex as the H_2O molecule (Figure 5). H_2O_2 is bound to the metal center by 7.2 kcal mol^{-1} (unbound by 0.8 kcal mol^{-1} without dispersion).

3.2.2. Deprotonation and Cleavage of H_2O_2. H_2O_2 protonates E202 (I9), and the hydrogen-bonding network is changed (I10), in the same manner as that in the first half-reaction (Scheme 3). In the second reductive half-reaction, the O−OH_2 bond is cleaved homolytically at a distance of 1.81 Å (TS2; Figure 4). The proton transfer from the base to the nonbridging oxygen atom occurs before the transition state. The manganese in site 1 (Mn1 in Figure 2) is redox-active,

dx.doi.org/10.1021/ic3008427 | Inorg. Chem. 2013, 52, 4173−4184

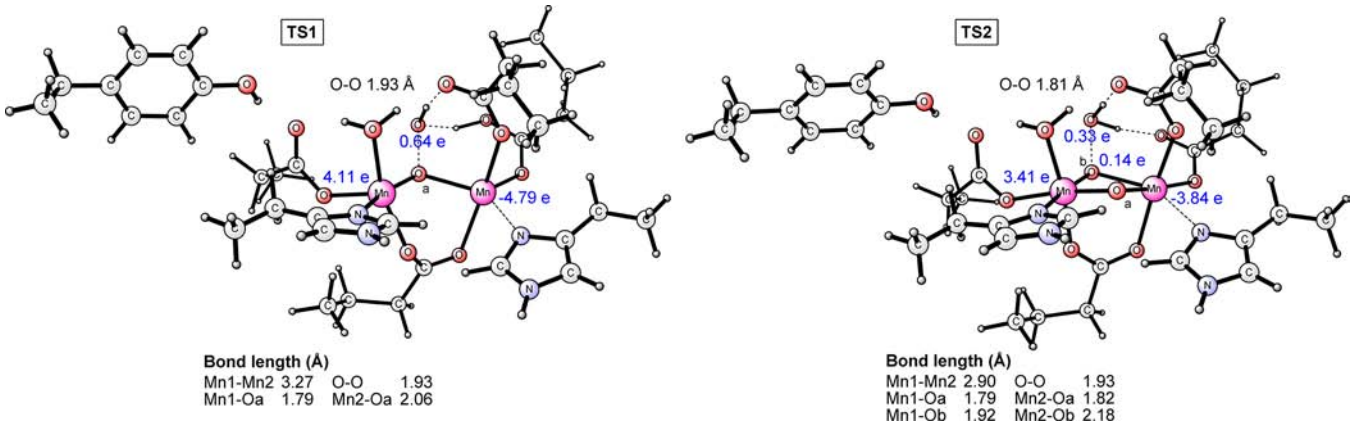

Figure 4. Structures and spin populations above 0.1 of the transition states for the first and second H_2O_2 reduction. Typical spin populations calculated with B3LYP in the metal dimers investigated are 4.8, 3.8, and 2.9 e for Mn(II), Mn(III), and Mn(IV), respectively.

Scheme 3. Proposed Reaction Scheme for the Second Reductive Half-Reaction[a]

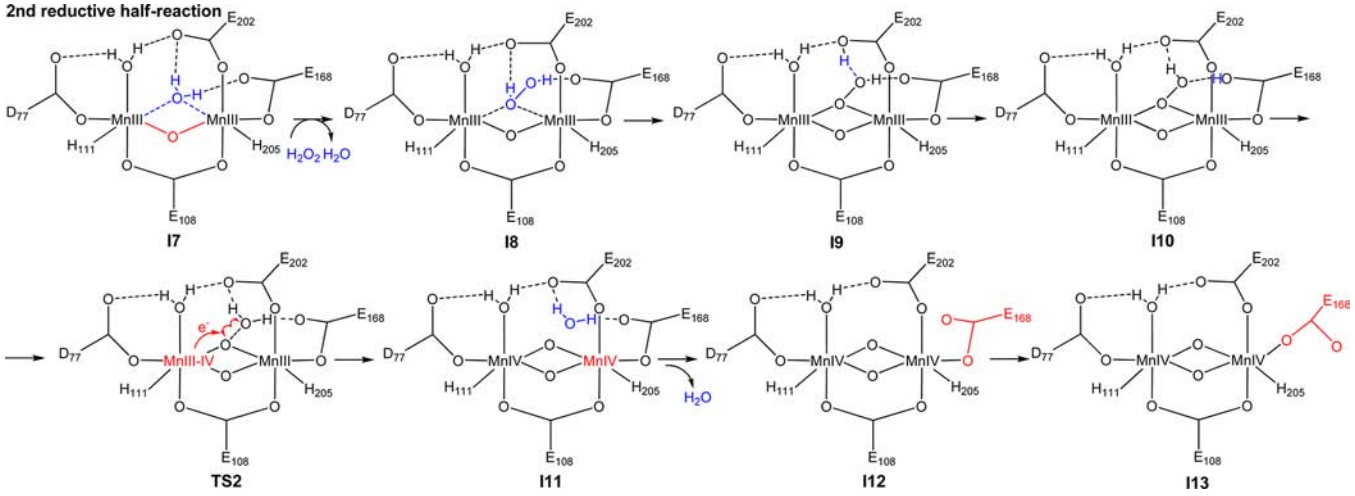

[a] *C. ammoniagenes* numbering.

being oxidized from Mn(III) to Mn(IV), and the electron is transferred to the bridging oxygen atom of O−OH_2. The reaction proceeds through an unstable Mn(IV)Mn(III) state with a H_2O cation radical. Because of the positive charge, an electron is attracted from the closest oxo bridge, and the radical is shared between H_2O and the bridge. The second electron transfer from the manganese in site 2 (Mn2 in Figure 2) is exergonic and without barrier, forming the product Mn(IV)-Mn(IV) state with a H_2O molecule (I11) (Figure 5).

The barrier is 17.0 kcal mol^{-1} (18.2 kcal mol^{-1} with the protonated model; Figure 5). The second-order rate constant for oxidation of R2c Mn(III)Fe(III) to Mn(IV)Fe(IV) by H_2O_2 is 8 ± 1 M^{-1} s^{-1} at 5 °C.[35] The barrier for H_2O_2 cleavage should be lower than 16 kcal mol^{-1}, corresponding to the apparent first-order rate constant at the highest measured concentration of H_2O_2 of 150 mM. In R2c, the redox-active metal in the transition state is most probably manganese because Mn(IV) has a lower redox potential than Fe(IV), or equivalently Mn(III) is easier to oxidize than Fe(III).[15,29]

The barrier for O−OH cleavage, when the reprotonation occurs after the transition state, is higher, 19.5 kcal mol^{-1}. The second reduction of H_2O_2 is less exergonic than the first reduction of H_2O_2 (Figure 3). The difference is due to the oxidation state of the metals, Mn(II)Mn(II) → Mn(III)Mn-(III) in the first half-reaction and Mn(III)Mn(III) → Mn(IV)Mn(IV) in the second half-reaction, and the number of bridging oxo species.

3.2.3. Mn(IV)Mn(IV) Product. In the Mn(IV)Mn(IV) state, the H_2O molecule formed is slightly unbound by 0.4 kcal mol^{-1} (by 5.4 kcal mol^{-1} without dispersion) and is released (Figure 5). The bis(μ-oxo) Mn(IV)Mn(IV) product state is 3.9 kcal mol^{-1} more stable when the glutamate E168 rotates to the position that is found in the X-ray crystal structure of oxidized manganese-dependent R2F from *C. ammoniagenes* (I13) (Figure 1). In the protonated model, proton transfer from D77 to one of the oxo bridges is favorable ($I13p_a$ to I13p) (Figure 5).

3.3. Formation of the Tyrosyl Radical. From the Mn(IV)Mn(IV) state, formation of a tyrosyl radical is exergonic with 2.3 kcal mol^{-1} (Figure 6A). The product is a Mn(III)-Mn(IV) state with a tyrosyl radical (I17) (Scheme 4). The state with Mn(III) in site 1 and Mn(IV) in site 2 (Mn1 and Mn2 in Figure 2) has a 2.9 kcal mol^{-1} lower calculated energy than the opposite assignment. The experimentally observed tyrosyl radical in manganese-dependent R2F from *C. ammoniagenes* is coupled to a ferromagnetically coupled Mn(III)Mn(III) state,[8] hence reduced by one more electron. The extra electron is in *E. coli* class Ia R2 provided by a neighboring tryptophan.[64,65] A

dx.doi.org/10.1021/ic3008427 | *Inorg. Chem.* 2013, 52, 4173−4184

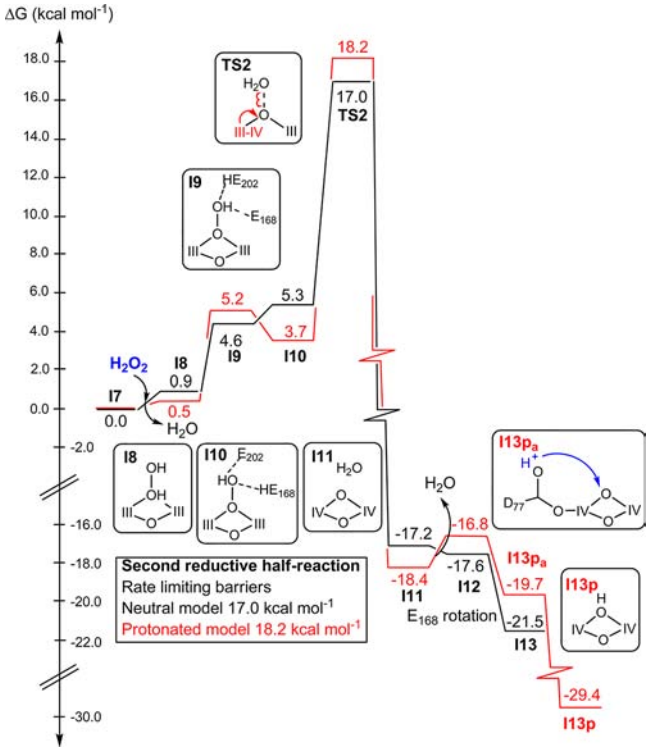

Figure 5. Energy profile for the second reductive half-reaction with a neutral model (black line) and a model in which D77 is protonated (red line). All values include solvation effects, zero-point corrections, empirical entropy corrections, and dispersion corrections. *C. ammoniagenes* numbering.

tryptophan residue has been identified in R2F from *C. ammoniagenes* in a similar structural position.[8] Formation of the tyrosyl radical from a Mn(III)Mn(IV) state, where one electron and one proton have been added, is thermoneutral, +0.6 kcal mol^{-1} (Figure 6B). The corresponding ferromagnetic state with a tyrosyl radical has a 0.7 kcal mol^{-1} lower energy and can easily be formed from the antiferromagnetic state. Hence, both the Mn(IV)Mn(IV) and Mn(III)Mn(IV) states are of sufficient potential to oxidize the tyrosine. The calculated proton-coupled redox potential of the Mn(IV)Mn(IV) state is slightly higher than that for the Mn(III)Mn(IV)-Y$^{\bullet}$ state with 2.9 kcal mol^{-1}, suggesting that an extra electron might be transferred from the tryptophan before tyrosyl-radical formation. However, the energy difference is not high enough to exclude an electron transfer after tyrosyl-radical formation. The extra electron may also be transferred from the tryptophan already before or during the second cleavage of H_2O_2, in which case the Mn(IV)Mn(IV) state would never be formed. This slightly different reaction mechanism could be investigated further in the future.

The proton-coupled electron transfer from the tyrosine to the metal center can be mediated by D77. However, the first intermediate in the radical formation, with a tyrosyl radical and protonated D77, is energetically highly unfavorable, when the metals are in both a Mn(III)Mn(IV) state [radical formation from Mn(IV)Mn(IV)] and a Mn(III)Mn(III) state [radical formation from Mn(III)Mn(IV)]. If instead there is first proton transfer mediated by E202 from the terminal H_2O bound to the manganese in site 2 (Mn2 in Figure 2) to one oxo bridge, proton transfer from the tyrosine to the metal center is faster (Scheme 4). The highest intermediate along this reaction pathway is 13.0 kcal mol^{-1} from Mn(IV)Mn(IV) (I16) and 17.0 kcal mol^{-1} from Mn(III)Mn(IV) (I16ep) (Figure 6A,B).

In the protonated model, formation of Tyr$^{\bullet}$ from a positively charged Mn(IV)Mn(IV) state (I13p) is exergonic with 4.9 kcal mol^{-1}, and there are no high-lying intermediates. The same positively charged Mn(IV)Mn(IV) state could also be formed if a proton and no electron is added to the neutral Mn(IV)Mn(IV) state (I13). Hence, the protonated Mn(IV)Mn(IV) state is of sufficient potential to oxidize the tyrosine. However, the cost of adding the proton, either to the neutral Mn(IV)Mn(IV)

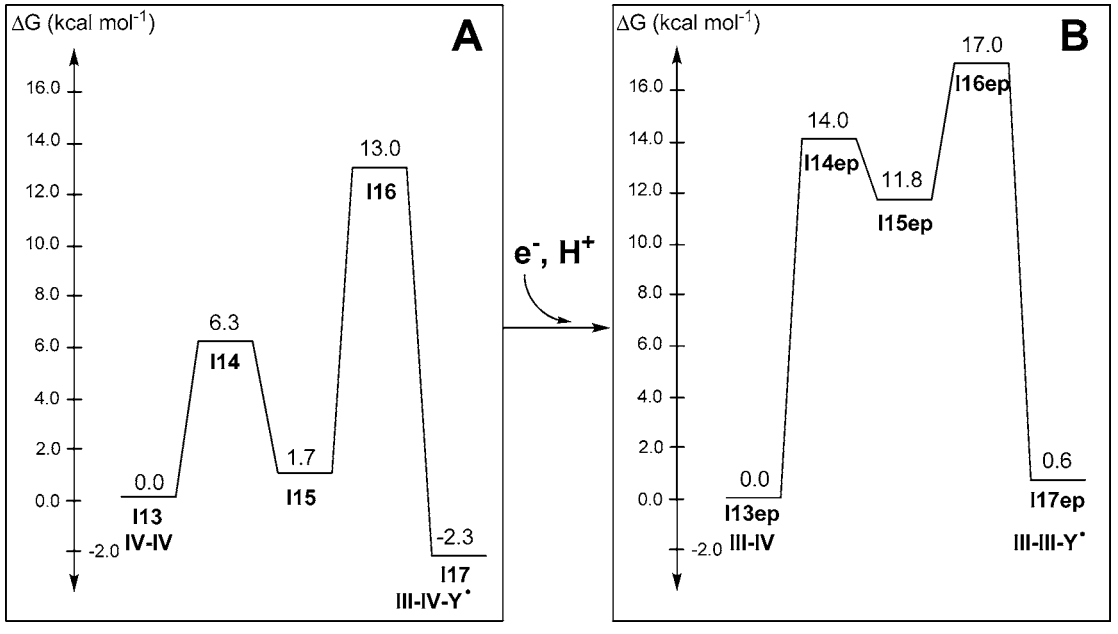

Figure 6. Energy profile for tyrosyl-radical formation from the (A) Mn(IV)Mn(IV) and (B) Mn(III)Mn(IV) states. All values include solvation effects, zero-point corrections, empirical entropy corrections, and dispersion corrections.

dx.doi.org/10.1021/ic3008427 | Inorg. Chem. 2013, 52, 4173−4184

Scheme 4. Proposed Reaction Scheme for Tyrosyl-Radical Formation[a]

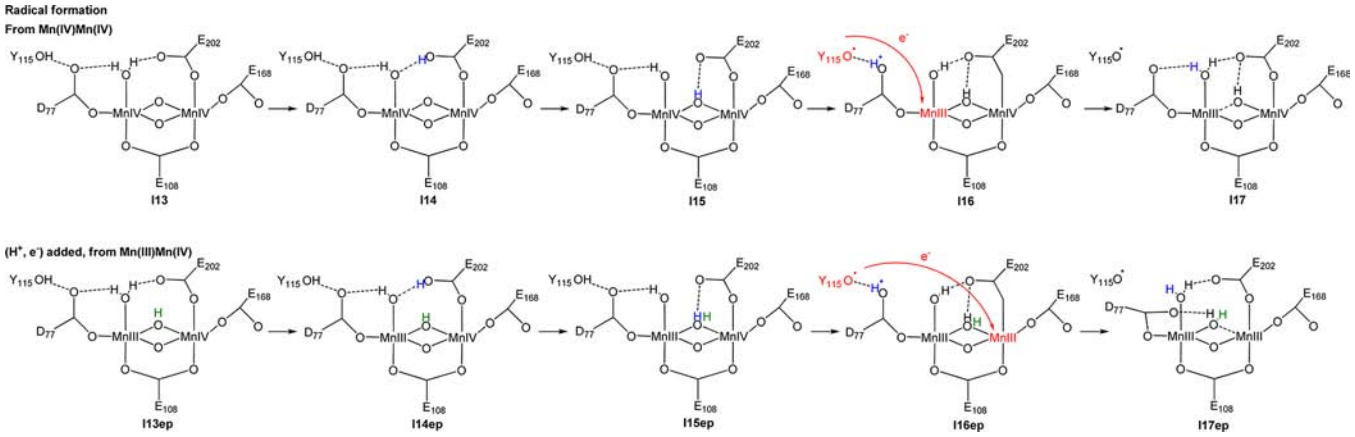

[a] *C. ammoniagenes* numbering.

Scheme 5. Key Intermediates and Energies for the Second Reductive Half-Reaction in R2F Compared to an Oxidative Half-Reaction Similar to the One of MnCat[a]

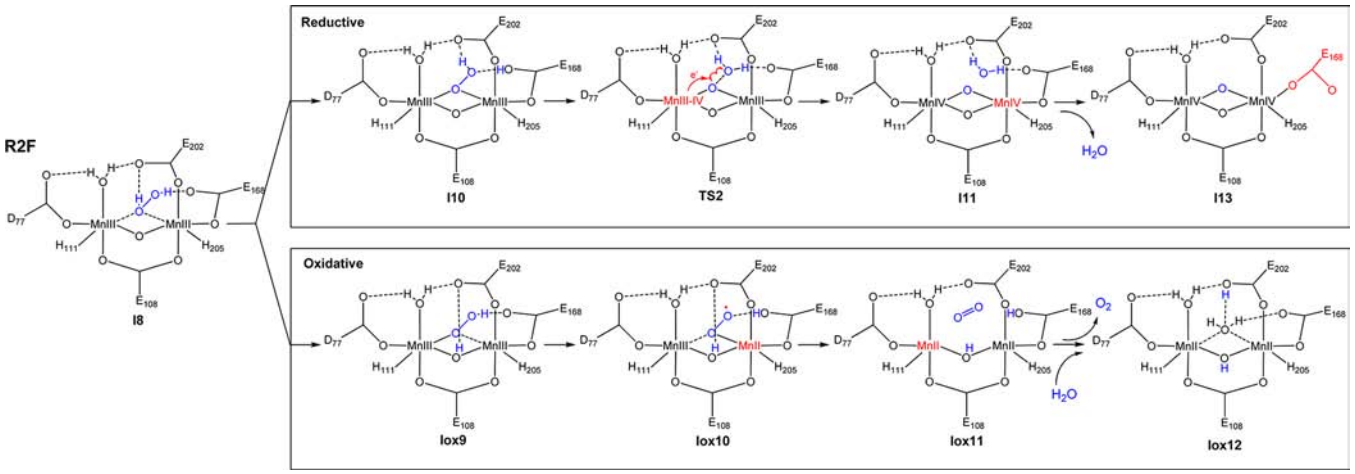

[a] *C. ammoniagenes* numbering.

state or upon formation of the model with protonated D77, has to be taken into account for a complete picture.

If HO_2^- is the oxidant, the product after the second reductive half-reaction could be a negatively charged Mn(IV)Mn(IV) state with one less proton. However, in this case, formation of $Tyr^\bullet$ is endergonic with 7.9 kcal mol^{-1}. Hence, if HO_2^- is the oxidant, the reaction should be coupled to proton uptake. From a negative Mn(III)Mn(IV) state, where only one electron and no proton has been taken up, formation of the tyrosyl radical is endergonic with 3.4 kcal mol^{-1}. Hence, electron uptake from the tryptophan should be coupled to proton uptake in order for tyrosyl-radical formation to be favorable.

3.4. Comparison with MnCat. Instead of the proposed second reductive half-reaction in R2F, in MnCat there is an oxidative half-reaction, where H_2O_2 is oxidized, forming oxygen (Scheme 5). It has been suggested that the dismutation reaction is avoided in R2F because E202 is opened up from a bridging binding mode in the Mn(II)Mn(II) reduced state to a monodentate mode in the Mn(III)Mn(III) state. In the monodentate mode, E202 is suggested to be too far from the peroxide, and therefore no longer a possible base.[8] However, as shown in the present work, a monodentate E202 can still reach the peroxide and act as a base in the reductive reaction.

The reason why R2F does not catalyze the dismutation reaction must be another one. The dismutation reaction in R2F has been modeled. The pathway for an oxidative reaction might be kinetically possible (Figure 7). However, the most stable product Mn(II)Mn(II) state (Iox12) has almost the same energy as that of the reactant Mn(III)Mn(III) state with bound H_2O_2 (I8). The reaction is thus thermoneutral and should be reversible. The competing reductive reaction where H_2O_2 is reduced is highly exergonic with 21.5 kcal mol^{-1} and hence irreversible (Figure 7). So, even though oxidation of the second H_2O_2 is possible, in the absence of additional H_2O_2, the reaction should be reversible, and eventually the reaction will proceed along the energy profile of the reduction, forming the oxidized Mn(IV)Mn(IV) state (I13) (Figure 7). If however, additional H_2O_2 is added fast enough to the product after the oxidative reaction, the reaction can proceed along the energy profile of the first reductive half-reaction, which is exergonic and irreversible (Iox12 to I3 to I7 in Figures 7 and 3).

The barrier for the second reductive half-reaction of 17.0 kcal mol^{-1} corresponds to a rate constant of about 1 s^{-1} from transition state theory (the expected accuracy of 3−5 kcal mol^{-1} for computed relative energies corresponds to 2−3 orders of magnitude for the reaction rate constant). Hence, the

dx.doi.org/10.1021/ic3008427 | *Inorg. Chem.* 2013, 52, 4173−4184

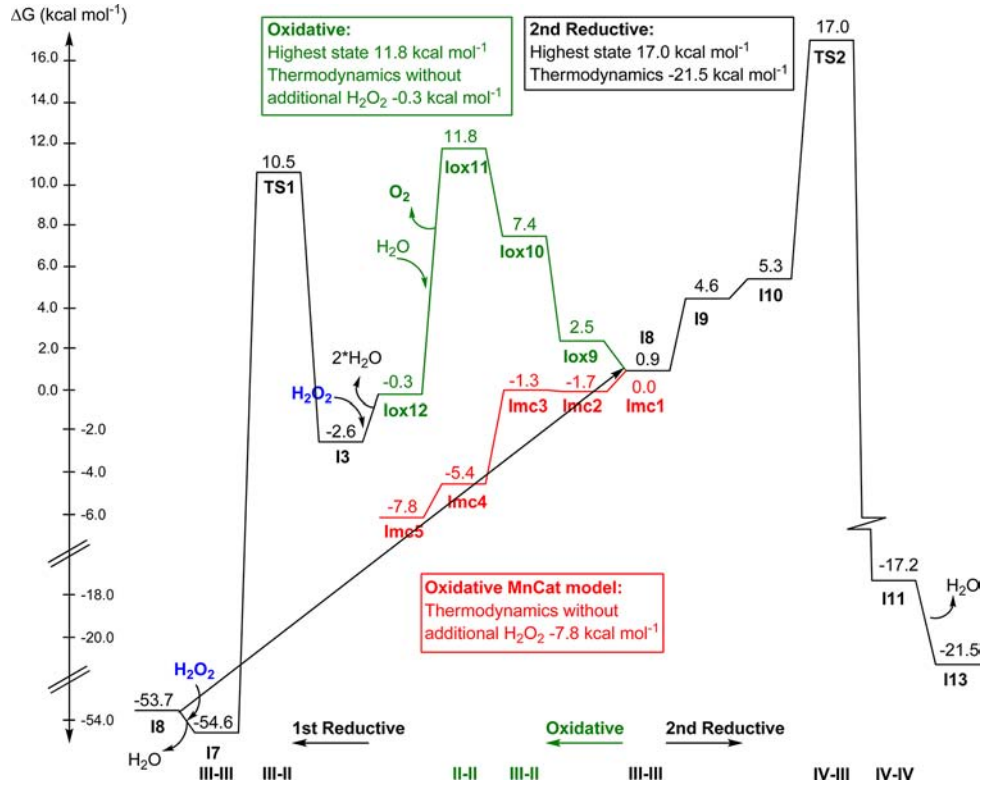

Figure 7. Energy profile for the second reductive half-reaction in R2F compared to an oxidative half-reaction similar to the one of MnCat. All values include solvation effects, zero point corrections, empirical entropy corrections and dispersion corrections. *C. ammoniagenes* numbering.

Scheme 6. Key Intermediates and Energies for the Oxidative Half-Reaction in MnCat, Based on a Model of R2F without E202 and with an Extra Hydroxo Bridge[a]

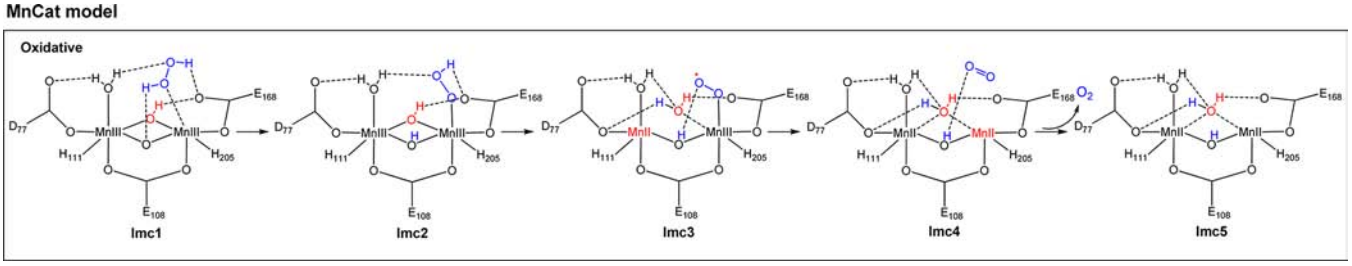

[a] *C. ammoniagenes* numbering.

calculations suggest that if additional H_2O_2 is available at a rate faster than 1 s^{-1}, there should be dismutation, while if additional H_2O_2 is available at a rate slower than 1 s^{-1}, the reaction should instead proceed along the second reductive half-reaction, forming the Mn(IV)Mn(IV) state and subsequently the tyrosyl radical.

In this context, one of the most important differences between MnCat and R2F is the number of coordinating carboxylates. In R2F, glutamate E202 is coordinating to the manganese in site 2 (Mn2 in Figure 2). In MnCat from *L. plantarum*, the corresponding glutamate E178 is not coordinating to the metal site, and in MnCat from *T. thermophilus*, there is no corresponding glutamate (Figure 1).[38,66]

A simple model of MnCat was constructed by removing the glutamate E202 and adding a hydroxo bridge to the Mn(III)Mn(III) state (Imc1) (Scheme 6). With the hydroxo bridge that is present in MnCat, the neutral charge of the active center is retained when the negatively charged glutamate is removed. One extra hydroxo bridge can be considered as one less proton compared to the R2F model. From the MnCat model Mn(III)Mn(III) state with added H_2O_2 (Imc1), the oxidative reaction is exergonic with 7.8 kcal mol^{-1}, forming a Mn(II)Mn(II) state and O_2 (Imc5) (Figure 7).

The reductive reaction is still highly exergonic (23.3 kcal mol^{-1}), forming a Mn(IV)Mn(IV) state. The barrier for the reductive H_2O_2 cleavage should be of the same size as that in R2F, hence 17 kcal mol^{-1} or higher because H_2O_2 no longer binds in a bridging position and the hydrogen bond from E168 is no longer present to stabilize the transition state. The total barrier from the oxidative reaction Mn(II)Mn(II) product (Imc5) to the reductive reaction Mn(IV)Mn(IV) product (I13) should then be at least 24 kcal mol^{-1} (Figure 7). Hence, in MnCat, a more stable Mn(II)Mn(II) product state may ensure that the dismutation reaction occurs independently of the time scale of available H_2O_2. Because the Mn(III)Mn(III) state is observed and not the Mn(II)Mn(II) state, there must also be other differences between MnCat and R2F that affect the reactivity. However, the calculated stabilization of the Mn(II)-

dx.doi.org/10.1021/ic3008427 | Inorg. Chem. 2013, 52, 4173−4184

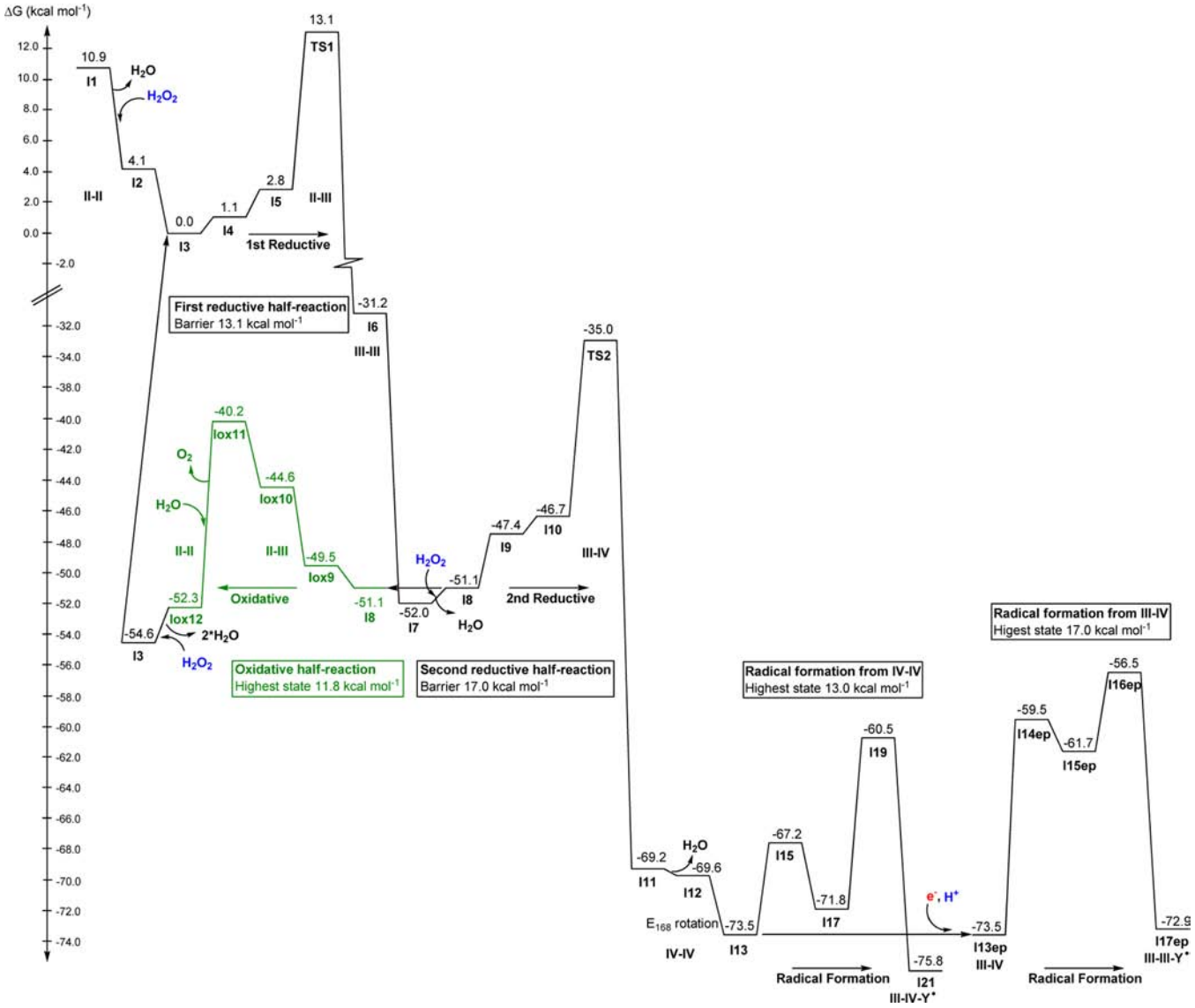

Figure 8. Energy profile for H_2O_2 cleavage and radical formation in class Ib R2F with a neutral model. All values include solvation effects, zero-point corrections, empirical entropy corrections, and dispersion corrections.

Mn(II) state in the simple MnCat model compared to that in R2F is one factor that may affect the selectivity between the dismutation reaction in MnCat and tyrosyl-radical formation in R2F.

The calculated higher exergonicity of the oxidative reaction in the MnCat model compared to the R2F model can be rationalized by the amount of available protons in the active site. In the oxidative reaction, two bases are needed to make O_2 from H_2O_2. In both the R2F and MnCat model, the oxo bridge can accept one proton, forming a hydroxo bridge. In the MnCat model, the additional hydroxo bridge can accept the second proton, forming H_2O (Imc5) (Scheme 6). In the R2F model, there is no additional hydroxo bridge, and glutamate E202 is instead accepting the second proton (Iox12) (Scheme 5). E202 in the R2F model is not as good a base as the additional hydroxo bridge in the MnCat model. The oxidative reaction may therefore be more exergonic in the MnCat model compared to the R2F model.

In R2F, destabilization of the Mn(II)Mn(II) state enables the possibility that the dismutation reaction may be avoided by slow uptake of H_2O_2. Speculatively, the role of NrdI may be to provide H_2O_2 oxidants in a controlled manner on the correct time scale. The observed inability of R2F to form the tyrosyl radical with the addition of H_2O_2 in the absence of NrdI[7,22] could then be due to too fast uptake of H_2O_2, leading to a dismutation reaction and hence catalase activity. This hypothesis should be possible to test experimentally.

The scenario described above is under the assumption that O_2 release in the oxidative reaction is faster than 1 s^{-1}, corresponding to the barrier for the second reductive half-reaction of 17 kcal mol^{-1}. If O_2 release is slower than 1 s^{-1}, the reaction would proceed to Mn(IV)Mn(IV) regardless of the rate of H_2O_2 addition. Because R2F is not activated by H_2O_2 in the absence of NrdI, another possibility is that NrdI is affecting the release of O_2, making it slower.

3.5. Observable Intermediates. From the calculated energy profile detailed in the previous sections, the scenario described below can be deduced. As a reminder, the expected accuracy of 3−5 kcal mol^{-1} for computed relative energies corresponds to 2−3 orders of magnitudes for the reaction rate

dx.doi.org/10.1021/ic3008427 | Inorg. Chem. 2013, 52, 4173−4184

constant. In the calculated energy profile for the whole activation reaction in R2F, there are three barriers: H_2O_2 cleavage in the first reductive half-reaction of 13.1 kcal mol^{-1}, H_2O_2 cleavage in the second reductive half-reaction of 17.0 kcal mol^{-1}, and formation of the tyrosyl radical from the oxidized state of 13.0 kcal mol^{-1} from Mn(IV)Mn(IV) or 17.0 kcal mol^{-1} from Mn(III)Mn(IV), where the second reductive half-reaction or radical formation from the Mn(III)Mn(IV) state should be the rate-limiting (Figure 8). The rate-limiting step could also be the addition of H_2O_2 from NrdI.

If H_2O_2 is delivered at a slower rate than 1 s^{-1} (corresponding to a barrier of 17.0 kcal mol^{-1}), either the rate-limiting step would be H_2O_2 addition, in which case the I1 Mn(II)Mn(II) and I7 Mn(III)Mn(III) intermediates should be possible to observe, or the rate-limiting step would be formation of the tyrosyl radical, in which case the I13ep Mn(III)Mn(IV) intermediate should be possible to observe.

If H_2O_2 is delivered at a faster rate than 1 s^{-1}, the dismutation reaction will occur. If H_2O_2 is delivered at a faster rate than 1 ms^{-1}, corresponding to the barrier for the first reductive half-reaction of 13.1 kcal mol^{-1}, the observed state in equilibrium would be I3 Mn(II)Mn(II).

If, on the other hand, H_2O_2 is delivered at a slower rate than 1 ms^{-1}, the observed states could be I7 Mn(III)Mn(III) and I8 Mn(III)Mn(III) or Iox12 Mn(II)Mn(II). If Iox12 is a few kilocalories per mole higher in energy, the only observed states (I7 and I8) would be Mn(III)Mn(III), in line with the observed oxidation of the cluster upon the addition of H_2O_2 to the reduced dimanganese *C. ammoniagenes* R2F, without NrdI.[22]

4. CONCLUSIONS

An energetically feasible reaction mechanism for activation of class Ib R2F by H_2O_2 has been suggested. The reaction proceeds through two reductive half-reactions. In the first half-reaction, H_2O_2 is cleaved with a barrier of 13.1 kcal mol^{-1}, and the dimanganese center is oxidized from Mn(II)Mn(II) to Mn(III)Mn(III). In the second half-reaction, the metal center is further oxidized from Mn(III)Mn(III) to Mn(IV)Mn(IV) and a second H_2O_2 is cleaved with a barrier of 17.0 kcal mol^{-1}. From an oxidized Mn(IV)Mn(IV) state, an electron can be taken up in combination with a proton, forming a Mn(III)Mn(IV) state. Tyrosyl-radical formation from both the Mn(IV)Mn(IV) and Mn(III)Mn(IV) states is both kinetically and thermodynamically accessible. Hence, chemically, H_2O_2 should be a possible oxidant for the manganese-dependent R2F. The reason why R2F cannot be activated by H_2O_2 without NrdI must be another one. (For example, changes in the structure leading to the inability of H_2O_2 to bind to the metal site, inability of H_2O_2 to enter into the active site, or competing reactions.) If HO_2^- is instead the oxidant, the reaction should be coupled to proton uptake in order for tyrosyl-radical formation to be favorable, resulting in the same product as if H_2O_2 is the oxidant. A model with protonated D77 as a starting point is from a kinetically perspective viable, but the possibility of formation of this state should depend on the pK_a of D77.

The selectivity between the second reductive half-reaction and a competing oxidative reaction, as in MnCat, may be the time scale of the available H_2O_2. If H_2O_2 is available at a faster time scale than 1 s^{-1}, corresponding to the rate-limiting barrier for the second reductive half-reaction, dismutation will occur. If H_2O_2 is available on a slower time scale than 1 s^{-1}, the second reductive half-reaction will occur, and the Mn(IV)Mn(IV) state and, subsequently, the tyrosyl radical will be formed. The role of NrdI may be to provide H_2O_2 on the correct time scale. In the absence of NrdI and in the presence of excess H_2O_2, the uptake may be too fast, leading to the dismutation reaction, and no tyrosyl-radical formation, as observed experimentally. This hypothesis could be investigated experimentally. In a model mimicking MnCat, the Mn(II)Mn(II) product of the dismutation reaction is stabilized. The more stable Mn(II)Mn(II) product state may ensure that the dismutation reaction occurs independent of the time scale of available H_2O_2. The more exergonic calculated oxidative reaction in the MnCat model compared to the R2F model can be rationalized by the additional hydroxo bridge in MnCat, which is a better base than the missing glutamate.

■ ASSOCIATED CONTENT

Ⓢ Supporting Information

Calculated relative energies of the reduced state when the backbone position of E168 is allowed to move, relative effects of adding dispersion corrections on the energy profile for the first reductive half-reaction, and coordinate file. This material is available free of charge via the Internet at http://pubs.acs.org.

■ AUTHOR INFORMATION

Corresponding Author

*E-mail: katarina.roos@fysik.su.se. Phone: +46 8 16 1268. Fax: +46 8 15 3679.

Notes

The authors declare no competing financial interest.

■ REFERENCES

(1) Jordan, A.; Reichard, P. *Annu. Rev. Biochem.* **1998**, *67*, 71−98.
(2) Nordlund, P.; Reichard, P. *Annu. Rev. Biochem.* **2006**, *75*, 681−706.
(3) Sjöberg, B. In *Metal Sites in Proteins and Models*; Hill, H., Sadler, P., Thomson, A., Eds.; Springer: Berlin/Heidelberg, 1997; Vol. *88*, pp 139−173.
(4) Stubbe, J. *Curr. Opin. Chem. Biol.* **2003**, *7*, 183−188.
(5) Högbom, M. *Metallomics* **2011**, *3*, 110−120.
(6) Cotruvo, J. A.; Stubbe, J. *Annu. Rev. Biochem.* **2011**, *80*, 733−767.
(7) Cotruvo, J. A.; Stubbe, J. *Biochemistry* **2010**, *49*, 1297−1309.
(8) Cox, N.; Ogata, H.; Stolle, P.; Reijerse, E.; Auling, G.; Lubitz, W. *J. Am. Chem. Soc.* **2010**, *132*, 11197−11213.
(9) Roshick, C.; Iliffe-Lee, E. R.; McClarty, G. *J. Biol. Chem.* **2000**, *275*, 38111−38119.
(10) Högbom, M.; Stenmark, P.; Voevodskaya, N.; McClarty, G.; Gräslund, A.; Nordlund, P. *Science* **2004**, *305*, 245−248.
(11) Jiang, W.; Yun, D.; Saleh, L.; Barr, E. W.; Xing, G.; Hoffart, L. M.; Maslak, M.-A.; Krebs, C.; Bollinger, J.; Martin, J. *Science* **2007**, *316*, 1188−1191.
(12) Voevodskaya, N.; Lendzian, F.; Ehrenberg, A.; Gräslund, A. *FEBS Lett.* **2007**, *581*, 3351−3355.
(13) Jiang, W.; Hoffart, L. M.; Krebs, C.; Bollinger, J. M. *Biochemistry* **2007**, *46*, 8709−8716.
(14) Jiang, W.; Saleh, L.; Barr, E. W.; Xie, J.; Gardner, M. M.; Krebs, C.; Bollinger, J. M. *Biochemistry* **2008**, *47*, 8477−8484.
(15) Roos, K.; Siegbahn, P. E. M. *Biochemistry* **2009**, *48*, 1878−1887.
(16) Sjöberg, B.-M. *Science* **2010**, *329*, 1475−1476.
(17) Auling, G.; Thaler, M.; Diekmann, H. *Arch. Microbiol.* **1980**, *127*, 105−114.
(18) Schimpff-Weiland, G.; Follmann, H. *Biochem. Biophys. Res. Commun.* **1981**, *102*, 1276−1282.
(19) Willing, A.; Follman, H.; Auling, G. *Eur. J. Biochem.* **1988**, *170*, 603−611.
(20) Fieschi, F.; Torrents, E.; Toulokhonova, L.; Jordan, A.; Hellman, U.; Barbe, J.; Gibert, I.; Karlsson, M.; Sjöberg, B.-M. *J. Biol. Chem.* **1998**, *273*, 4329−4337.

(21) Högbom, M.; Huque, Y.; Sjöberg, B.-M.; Nordlund, P. *Biochemistry* **2002**, *41*, 1381−1389.
(22) Huque, Y.; Fieschi, F.; Torrents, E.; Gibert, I.; Eliasson, R.; Reichard, P.; Sahlin, M.; Sjöberg, B.-M. *J. Biol. Chem.* **2000**, *275*, 25365−25371.
(23) Cotruvo, J. A.; Stubbe, J. *Biochemistry* **2011**, *50*, 1672−1681.
(24) Martin, J. E.; Imlay, J. A. *Mol. Microbiol.* **2011**, *80*, 319−334.
(25) Stolle, P.; Barckhausen, O.; Oehlmann, W.; Knobbe, N.; Vogt, C.; Pierik, A. J.; Cox, N.; Schmidt, P. P.; Reijerse, E. J.; Lubitz, W.; Auling, G. *FEBS J.* **2010**, *277*, 4849−4862.
(26) Abbouni, B.; Oehlmann, W.; Stolle, P.; Pierik, A. J.; Auling, G. *Free Radical Res.* **2009**, *43*, 943−950.
(27) Zhang, Y.; Stubbe, J. *Biochemistry* **2011**, *50*, 5615−5623.
(28) Crona, M.; Torrents, E.; Røhr, Å. K.; Hofer, A.; Furrer, E.; Tomter, A. B.; Andersson, K. K.; Sahlin, M.; Sjöberg, B.-M. *J. Biol. Chem.* **2011**, *286*, 33053−33060.
(29) Roos, K.; Siegbahn, P. *J. Biol. Inorg. Chem.* **2011**, *16*, 553−565.
(30) Roca, I.; Torrents, E.; Sahlin, M.; Gibert, I.; Sjöberg, B.-M. *J. Bacteriol.* **2008**, *190*, 4849−4858.
(31) Boal, A. K.; Cotruvo, J. A.; Stubbe, J.; Rosenzweig, A. C. *Science* **2010**, *329*, 1526−1530.
(32) Røhr, Å. K.; Hersleth, H.-P.; Andersson, K. K. *Angew. Chem., Int. Ed.* **2010**, *49*, 2324−2327.
(33) Johansson, R.; Torrents, E.; Lundin, D.; Sprenger, J.; Sahlin, M.; Sjöberg, B.-M.; Logan, D. T. *FEBS J.* **2010**, *277*, 4265−4277.
(34) Cotruvo, J. A.; Stubbe, J. *Proc. Natl. Acad. Sci.* **2008**, *105*, 14383−14388.
(35) Jiang, W.; Xie, J.; Nørgaard, H.; Bollinger, J. M.; Krebs, C. *Biochemistry* **2008**, *47*, 4477−4483.
(36) Dismukes, G. C. *Chem. Rev.* **1996**, *96*, 2909−2926.
(37) Boelrijk, A. E. M.; Dismukes, G. C. *Inorg. Chem.* **2000**, *39*, 3020−3028.
(38) Barynin, V. V.; Whittaker, M. M.; Antonyuk, S. V.; Lamzin, V. S.; Harrison, P. M.; Artymiuk, P. J.; Whittaker, J. W. *Structure* **2001**, *9*, 725−738.
(39) *Jaguar*, version 7.6; Schrodinger LLC: New York, 2009.
(40) Becke, A. D. *J. Chem. Phys.* **1993**, *98*, 5648−5652.
(41) Reiher, M.; Salomon, O.; Artur Hess, B. *Theor. Chem. Acc.* **2001**, *107*, 48−55.
(42) Siegbahn, P. E. M.; Blomberg, M. R. A. *Annu. Rev. Phys. Chem.* **1999**, *50*, 221−249.
(43) Salomon, O.; Reiher, M.; Hess, B. A. *J. Chem. Phys.* **2002**, *117*, 4729−4737.
(44) Hay, P. J.; Wadt, W. R. *J. Chem. Phys.* **1985**, *82*, 299−310.
(45) Dunning, T. H., Jr. *J. Chem. Phys.* **1989**, *90*, 1007−1023.
(46) Kendall, R. A.; Dunning, T. H., Jr.; Harrison, R. J. *J. Chem. Phys.* **1992**, *96*, 6796−6806.
(47) Woon, D. E.; Dunning, T. H., Jr. *J. Chem. Phys.* **1993**, *98*, 1358−1371.
(48) Tannor, D. J.; Marten, B.; Murphy, R.; Friesner, R. A.; Sitkoff, D.; Nicholls, A.; Honig, B.; Ringnalda, M.; Goddard, W. A. *J. Am. Chem. Soc.* **1994**, *116*, 11875−11882.
(49) Marten, B.; Kim, K.; Cortis, C.; Friesner, R. A.; Murphy, R. B.; Ringnalda, M. N.; Sitkoff, D.; Honig, B. *J. Phys. Chem.* **1996**, *100*, 11775−11788.
(50) Blomberg, M. R. A.; Siegbahn, P. E. M.; Babcock, G. T. *J. Am. Chem. Soc.* **1998**, *120*, 8812−8824.
(51) Frisch, M. J. et al. *Gaussian 03*, revision D.01; Gaussian, Inc.: Wallingford, CT, 2004.
(52) Kelly, C. P.; Cramer, C. J.; Truhlar, D. G. *J. Chem. Theory Comput.* **2005**, *1*, 1133−1152.
(53) O'Sullivan, D. W.; Lee, M.; Noone, B. C.; Heikes, B. G. *J. Phys. Chem.* **1996**, *100*, 3241−3247.
(54) Siegbahn, P. E. M. *Philos. Trans. R. Soc., B* **2008**, *363*, 1221−1228.
(55) Grimme, S. *J. Comput. Chem.* **2006**, *27*, 1787−1799.
(56) Sinnecker, S.; Neese, F.; Noodleman, L.; Lubitz, W. *J. Am. Chem. Soc.* **2004**, *126*, 2613−2622.
(57) Siegbahn, P. E.; Himo, F. *Wiley Interdiscip. Rev., Comput. Mol. Sci.* **2011**, *1*, 323−336.
(58) Hopmann, K. H.; Himo, F. *J. Chem. Theory Comput.* **2008**, *4*, 1129−1137.
(59) Georgieva, P.; Himo, F. *J. Comput. Chem.* **2010**, *31*, 1707−1714.
(60) Sevastik, R.; Himo, F. *Bioorg. Chem.* **2007**, *35*, 444−457.
(61) Rong-Zhen, L.; Jian-Guo, Y.; Fahmi, H. *J. Chem. Theory Comput.* **2011**, *7*, 1494−1501.
(62) Hu, L.; Eliasson, J.; Heimdal, J.; Ryde, U. *J. Phys. Chem. A* **2009**, *113*, 11793−11800.
(63) Sumowski, C. V.; Ochenfeld, C. J. *J. Phys. Chem. A* **2009**, *113*, 11734−11741.
(64) Baldwin, J.; Krebs, C.; Ley, B. A.; Edmondson, D. E.; Huynh, B. H.; Bollinger, J. M. *J. Am. Chem. Soc.* **2000**, *122*, 12195−12206.
(65) Pötsch, S.; Lendzian, F.; Ingemarson, R.; Hörnberg, A.; Thelander, L.; Lubitz, W.; Lassmann, G.; Gräslund, A. *J. Biol. Chem.* **1999**, *274*, 17696−17704.
(66) Antonyuk, S.; Melik-Adamyan, V.; Popov, A.; Lamzin, V.; Hempstead, P.; Harrison, P.; Artymyuk, P.; Barynin, V. *Crystallogr. Rep.* **2000**, *45*, 105−116.